Computational modeling of the bacterial 70S ribosome and its subunits

Joanna Trylska

Interdisciplinary Centre for Mathematical and Computational Modelling, University of Warsaw, Warsaw

Computational modeling of the bacterial 70S ribosome and its subunits

Summary

The computational modeling studies performed on the entire 70S bacterial ribosome and its subunits are reviewed. Computational approaches became possible with the availability of three-dimensional atomic resolution structures of the ribosomal subunits. However, due to enormous size of the system theoretical efforts to study the ribosome are few and still pose a great challenge. For example, to extend the simulation time scales to biologically relevant ones, often reduced models requiring tedious parameterization procedures need to be applied. So far modeling of the ribosome involved its electrostatic properties, internal dynamics, binding of antibiotics, polypeptide folding in the ribosome tunnel, and assembly paths of proteins in the small ribosomal subunit.

Key words:
70S ribosome, 30S subunit, molecular modeling, electrostatics, internal dynamics.

Address for correspondence

Joanna Trylska,
Interdisciplinary Centre
for Mathematical
and Computational
Modelling,
University of Warsaw,
Zwirki i Wigury St. 93,
02-089 Warsaw,
Poland;
e-mail:
joanna@icm.edu.pl

biotechnologia
1 (84) 36–47 2009

1. Introduction

Ribosome is a nanoscale ribonucleoprotein complex responsible for the process of translation in the cell. It is composed of two subunits which in bacteria are denoted 30S and 50S in accord with their sedimentation coefficients. The two subunits associate through a network of interactions to form the 70S active bacterial ribosome (see Fig.). The 50S subunit in bacteria conta-

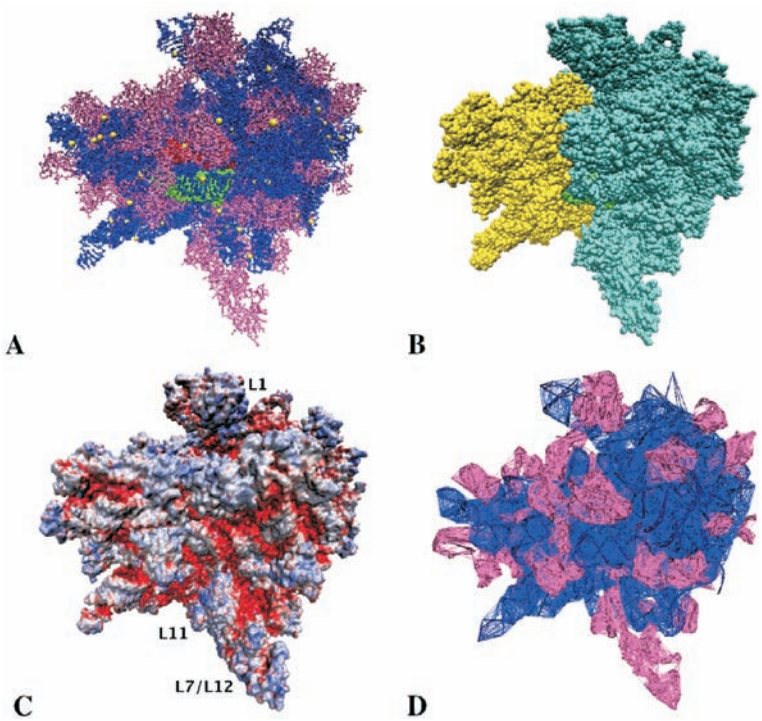

Fig. 70S *T. thermophilus* ribosome model based on the 1GIX and 1GIY crystal structures (5) and a homology model obtained in (13, 14). **A:** All-atomic model with proteins in magenta, ribosomal RNA in blue, A-site tRNA in green, P-site tRNA in red, Mg^{2+} ions in yellow. **B:** All-atomic van der Waals model with 30S subunit in yellow and 50S subunit in cyan. **C:** The electrostatic potential calculated for the all-atom ribosome and projected onto its molecular surface. The scale changes from red $\leqslant$ -5.0 kT/e, through white 0 kT/e to blue $\geqslant$ +5.0 kT/e. **D:** Coarse-grained elastic network model of the ribosome. The vertices denote P and Cα pseudo atoms and lines define the interactions.

ins over 30 proteins which are numbered and named beginning with the letter L to indicate they are from the large subunit. It also contains two ribosomal RNA sequences called 23S rRNA (~2904 nucleotides) and 5S rRNA (~120 nucleotides). The 30S subunit contains 21 proteins, a single 16S rRNA sequence (~1542 nucleotides), and it binds messenger RNA (mRNA). Proteins in the small subunit are also numbered and their names begin with the letter S.

Amino acids are brought to the ribosome by transfer RNAs (tRNAs). The ribosome comprises three tRNA binding sites located at the interface between subunits: A – aminoacyl, P – peptidyl and E – exit. The A-site accepts the incoming aminoacylated tRNA, the P-site holds the tRNA with the emerging peptide chain, and the E-site holds the deacylated tRNA before it leaves the ribosome. Peptide bond synthesis occurs between the aminoacyl and peptidyl ends of A-and P-site tRNAs in the so called peptidyl transferase center in the large subunit. After the reaction, tRNAs

must cooperatively translocate to their new positions (P and E) with the advance of mRNA by exactly one codon. The E-site tRNA is then ready to leave the ribosome and a new tRNA may bind in the A-site. The nascent polypeptide leaves the ribosome through a tunnel in the 50S subunit.

The events occurring in three distinct stages of bacterial translation (initiation, elongation, and termination) are modulated by the binding of various factors to the ribosome-e.g., by elongation factor Tu (EF-Tu) and elongation factor G (EF-G) in the elongation stage and release factors (RFs) in the termination stage. EF-Tu-GTP complexes with the aminoacyl-tRNA and delivers it to the A-site. When the appropriate charged tRNA is deposited into the A-site, the GTP is hydrolyzed, the A-tRNA is accommodated, and the EF-Tu-GDP is released. Next, EF-G associates and promotes the translocation of tRNAs and mRNA. The binding of these factors must be, therefore, very precise and must occur in exactly right phase of translation. Upon binding elongation factors were found to undergo large structural rearrangements (1).

Peptide synthesis in bacteria can be inhibited by many antibiotics that bind to specific sites (mainly RNA) in the ribosome (1). Some antibiotics prevent the association or dissociation of various factors, while others hinder the incorporation of tRNAs, inhibit functional conformational changes of the ribosome or prevent the nascent peptide from leaving the ribosome. For example, aminoglycosidic antibiotics bind to the 16S RNA in the 30S subunit and interfere with decoding. Bacteria develop resistance against various antibiotic classes; therefore computational modeling also focuses on the aspects of antibiotic-ribosome binding.

With the appearance in the year 2000 of the all-atom crystal structures of the 30S (2,3) and 50S subunits (4) and a year later of a 5.5Å resolution structure of the entire 70S ribosome (5), theoretical computational modeling of the ribosome became possible. This structural data deposited into the Protein Data Bank (6) provided great opportunities to examine by various simulation techniques structural, dynamical and electrostatic properties of the ribosome. Nevertheless, from the point of view of theoretical methods, modeling the entire ribosome or its subunits even though feasible, is still challenging due to the system size. The 30S subunit is composed of approximately 95 000 atoms and spans a box of $210 \times 180 \times 200$Å. The 50S subunit is even larger and consists of approximately 140 000 atoms. Altogether the bacterial ribosome has nearly 240 000 atoms not including the surrounding first-solvation shell water molecules or counter-ions and its overall dimensions are about 25 nm^3 .

2. Electrostatic properties of the ribosome

Electrostatics, due to its long-range nature, plays a key role in many biological processes. Because biomolecules are characterized by complicated charge distributions, electrostatics often dominates their inter- and intra-molecular interactions. Therefore, in theoretical studies of biomolecular properties, one of the important

aspects is a proper description of the electrostatic potential around molecules. The most common and successful approach used to obtain such electrostatic properties is the Poisson-Boltzmann theory (7,8). A molecule described by a set of fixed partial charges and radii is immersed in implicit solvent with ionic strength. The ionic concentrations are described by the Boltzmann distribution. To obtain the electrostatic potential the so called Poisson-Boltzmann equation is solved with numerical techniques on a three dimensional grid covering the molecule and its surrounding environment. The distance between the points of the grid defines the resolution of the calculation.

The first effort to determine the electrostatic potential around the entire 30S subunit arose due to the development of the Adaptive Poisson-Boltzmann Solver (9) (APBS). The software was designed to solve the Poisson-Boltzmann equation for large nanoscale systems. The authors calculated the electrostatic properties of all-atomic structures of the small and large ribosomal subunits. Calculations utilized 343 processors of the NPACI Blue Horizon supercomputer at San Diego Supercomputer Center what resulted in a grid resolution of 0.4Å. The electrostatic potential around the subunits was mainly negative due to the presence of negatively charged phosphate groups of RNA. Positive potential patches resulted from the ribosomal proteins and the presence of counterions. The potential surface maps between the subunit association sides showed qualitative electrostatic complementarities. The authors found that the codon binding sites are surrounded by positive potential regions which could aid the stabilization of tRNAs and mRNA. The proteins of the large subunit involved in tRNA binding also exhibit positive potential patches, especially around L44e, L5 and L10e.

It was shown that during translation the ribosome undergoes large-scale conformational changes that are relevant to its function (10,11). One of these changes is the ratchet-like movement of the subunits that takes place in the elongation stage of translation. Therefore, the next electrostatic study explored the changes in the electrostatic potential around the ribosome during the ratchet-like motion of the subunits (12). The first 5.5Å resolution (5) crystal structure of the entire ribosome was used and the conformations occurring during the ratcheting motion were derived from the normal mode analysis (see section Internal dynamics of the ribosome). Due to the availability of only low resolution structure of the 70S ribosome, a reduced electrostatics Poisson-Boltzmann model was developed. Based on all-atom electrostatic models of the 30S subunit effective partial charges and radii were parameterized and applied to the entire ribosome. The electrostatic potential around the ribosome is mainly negative due to the fact that two-thirds of the ribosomal mass arises from the RNA. However, positive patches of the electrostatic potential are found and come mainly from the positively charged proteins. Changes in the electrostatic potential along the ratchet-like displacement were observed mainly in the tRNA binding sites. Positive electrostatic potential was observed in the areas where the EF-G, EF-Tu and RFs bind. This study also showed the complementarities

of the long-range electrostatic potential between EF-G and its binding site. The L1 protein was found to be a source of positive potential, possibly facilitating the release of E-site tRNA from the ribosome. The peptidyl transferase center which is bare of proteins is characterized by a negative electrostatic potential. Large positive potential spots are associated mainly with proteins L6, L11, S12 and S19.

Recently all-atomic Poisson-Boltzmann calculations of the electrostatic potential became possible. The figure presents the electrostatic potential projected on the molecular surface of the entire 70S ribosome. Calculations were performed for the model of Sanbonmatsu et al. (13,14) that was based on the crystal structure of Yusupov et al. (5). The positions of divalent ions corresponded to experimental conditions of 7 mM $MgCl_2$ and were taken from the all-atom molecular dynamics simulations (14). The monovalent ionic strength was set to 150 mM. We also modeled the missing side-chains of L1, L2, L7/L12, L9, L11, L13, L16, L23 and L25 proteins and optimized their positions to avoid bad contacts. The all-atom derived electrostatic potential confirms the earlier potential maps derived for the reduced ribosome model. Many strongly negative patches are observed even though positive areas corresponding mainly to proteins do appear.

3. Binding of antibiotics to the 30S subunit

Blocking the bacterial ribosome function leads to inhibition of microbial growth, what is important in alleviating bacterial infections. Aminoglycoside antibiotics, positively charged sugar derivatives such as paromomycin and neamine, bind in the A-site of the 30S subunit and interfere with the decoding. They have also been found to interfere with the assembly of ribosomal subunits (15). Aminoglycosides were the first antibiotics to be crystallized in the complex with the 30S subunit, therefore, computational studies of their binding to the small subunit were initially performed for this class of antibiotics.

The first theoretical study to determine the energetics of binding of aminoglycosides to the entire 30S subunit was performed by Ma et al. (16). Total binding free energies were calculated based on the continuum solvation Poisson-Boltzmann model combined with the surface area-dependent nonpolar term and based on experimental data. The change in electrostatic term and the change in the solvent accessible surface area upon ligand binding to the 30S subunit were calculated to give the binding energy of the ligand. This so called PB/SASA model is popular and serves well in the studies of the energetics of binding (17). If a three dimensional structure of a ligand-macromolecule complex is known from structural experiments, energetics of binding of the ligand may be studied. Therefore, when the first structure of the 30S subunit in complex with aminoglycosides was solved, computational energetic studies were performed (16). The authors found reasonable correspondence with experimental data obtained for binding of aminoglycosides to a model A-site RNA.

Later, Yang et al. (18) extended the previous model by additionally estimating the entropy loss of aminoglycosidic rings upon binding, as well as the translational and rotational entropy changes. The parameters of the model for the 30S subunit were determined based on calculations for a smaller A-site oligonucleotide, as well as experimental studies. These studies have shown that, despite many approximations, the implicit solvent Poisson-Boltzmann model is amenable to investigating the overall binding hierarchy of antibiotics to the 30S subunit. Moreover, the model was able to perceive small charge perturbations caused by different functional groups in the antibiotic rings.

By means of Brownian Dynamics, we have recently investigated the rates of binding of paromomycin to the whole 30S subunit (19). We found that the antibiotic first diffuses toward the subunit and then explores the surface to encounter the A-site. During the pathway leading to binding in the A-site it also interacts with other possible cavities that are binding sites for other antibiotics.

4. Internal dynamics of the ribosome

By means of cryo-electron microscopy it was shown that the ribosome is a very dynamic machine (10,11). For example, a ratchet-like motion of the subunits related to translocation of tRNAs and mRNA was found (11). It was also postulated that translocation involves a significant movement of the L1 stalk (20).

The global motions of the ribosome based on the 25Å cryo-electron microscopy density maps and elastic network models were studied (21). The elastic net was constructed from the electron density map. The interactions were defined as harmonic Hookean springs which means that they varied quadratically around the potential energy minimum but it was found earlier that molecules often behave as if their energy surface was parabolic. Normal mode analysis was applied to derive the lowest-frequency vibrational modes. The ratchet-like motion of the 30S relative to the 50S subunit was observed. This fact suggested that this movement is an inherent property of the shape of the ribosome that can be treated as an elastic body. Global motions depend on the global shape and character of deformations and not on the details of the potential energy function and they often correspond to functional motions.

A more detailed study applied normal mode analysis to explore the internal dynamics of the ribosome based on the 5.5Å resolution crystal structure (22,23). In this model only phosphate and Cd carbon atoms were considered. The system was represented as an elastic network see (Fig.) and the lowest frequency modes were characterized. It turned out that those modes include the ratchet-like relative motion of the subunits. Moreover, displacements of the L1 ribosomal stalk, opening and closing the intersubunit space near the E-site was observed. The L11 protuberance on the other side of the ribosome also exhibited a large scale motion.

In normal mode analysis harmonic potentials are applied and the motions can only be characterized separately one at a time. Therefore, to overcome this drawback and to increase the level of detail of the dynamics, a reduced molecular dynamics simulation of the ribosome was performed, which accounted as well for some anharmonicity of motions (12). The extension of the elastic network model (Fig.) included all-atom like potential energy function, which distinguished both local bonded and non-local non-bonded interactions. The parameterization was based on pair distribution functions, derived from the low-resolution crystal structure of the ribosome (5). Half a microsecond molecular dynamics simulation time scales were achieved. This study found that the movements of L7/L12 and L1 lateral stalks are anti-correlated and span a range up to 15Å. Ratchet-like rotation of the subunits correlated with the movement of the L1 stalk was also observed. The 50S subunit was found to undergo many local internal fluctuations and the 30S subunit was more compact and moving as one uniform block. The tRNA CCA-3' termini and anticodons exhibited small fluctuations, which suggests tight alignment of substrates during the formation of peptide bond and decoding.

The above reduced modeling of the internal dynamics of the ribosome has proven that the ribosome internal mobility arises due to its shape and is inherent to the system. Global functional motions and rearrangements are therefore only accelerated by GTP. It was found that translation is possible without GTP hydrolysis and can indeed be factor-free (24,25), so the studies were in accord with experimental data.

In the year 2005 Sanbonmatsu et al. (14) published the first all-atom molecular dynamics simulation of the entire ribosome in explicit solvent, which focused on the incorporation of tRNA into the ribosomal A-site. As the initial configuration, the all-atom homology model of the *Thermus thermophilu*s 70S ribosome was used (13), with the entire simulation box consisting of 2.64 million atoms. Molecular dynamics were performed at Los Alamos National Laboratory ASCI Q-machine supercomputer, using 512, 768, and 1024 processors and about 10^6 computer hours. The overall time scale of the simulation was about 20 ns. The authors simulated the accommodation of aminoacyl-tRNA with many 2ns long targeted molecular dynamics runs by gradually reducing the root mean square deviation of the starting structure toward the final A-tRNA configuration. Recently, all-atom molecular dynamics simulations of the 30S ribosomal subunit based on the 1J5E structure including 1.07 million atoms were also performed (26).

5. Ribosome tunnel

Before the release from the ribosome, the newly synthesized polypeptide travels through a 100Å long tunnel in the 50S subunit. The lateral dimensions of the tunnel are between 10 and 20Å and its walls are made mainly of ribosomal RNA. The tunnel

is believed to provide a constrained environment for co-translational folding, especially in case of α helices. An exemplary experimental study (27) found that the structure formation can occur inside the ribosome but it can depend on the location within the tunnel and the length of the nascent chain. It seems that it can also depend on the sequence and native structure of the protein.

Coarse-grained Langevin dynamics simulations of polypeptide folding in the tunnel modeled as a cylinder were performed (28). It was found that such confinement can indeed entropically stabilize α-helices (28), because the diameter of the tunnel is close to that of an α-helix. Longer helices were more stabilized than short ones.

Translocation of the β-hairpin-forming peptide through a tunnel that mimics the one in the ribosome was also studied (29). The protein was represented in a coarse-grained manner and its movement *via* a cylindrical tunnel was also modeled with Langevin dynamics. The authors have found, that when the diameter of the tunnel decreases below a certain value of about 13.7Å, the protein assumes an extended configuration. In a wider tunnel the protein is stabilized in the folded state.

However, Adrian Elcock (30), who studied the path of the peptide through the ribosome tunnel with a Go-like folding model (31), found that confinement of the emerging polypeptide does not necessarily promote formation of the native structure during synthesis. Three model proteins were studied: chymotrypsin inhibitor 2, barnase and Semliki forest virus protein. Amino acids were gradually added at the ribosome peptidyl transfer center and according to Brownian dynamics protocol, their movement through the large subunit tunnel was generated. The large subunit was represented at a near-atomic level and the nascent proteins with only Cα carbons. Simple confinement of the protein within the tunnel did not significantly affect its folding.

Therefore, more studies are needed to determine the influence of the ribosome tunnel on the folding of synthesized polypeptides.

6. Assembly of the subunits

The assembly of the ribosome and its subunits is a complicated process that can spontaneously occur under certain conditions also *in vitro*. This means that all the information required for the proper assembly is present only in the RNA and protein components. The assembly of the 30S subunit was found to be a sequential and cooperative process. The first experimental small subunit assembly map was determined by Held et al. (32). It classified the proteins into three groups: primary binders, the ones that could bind to the bare 16S RNA; secondary binders – could bind only after one of the primary proteins was bound; and tertiary proteins – could bind only after at least one primary and at least one secondary protein were bound. In 1993 Powers et al. (33) presented a kinetics based 30S assembly map derived from chemical foot-printing studies. The map classified proteins into early, middle,

middle-late and late binders, and suggested that assembly proceeds roughly from the 5' to 3' end of 16S RNA. The kinetics assembly landscape, predicting by mass-spectrometry techniques the association rate constants for individual proteins, was also determined in (34). A nice review of the 30S subunit assembly biophysical studies is provided by James Williamson (35).

The 16S RNA can be divided into three individual domains: 5', central, and 3' and the crystal structures have shown that majority of the 30S proteins interact exclusively with individual 16S RNA domains. The above experimental studies indicated few pathways in the assembly process, corresponding to the 16S RNA domains, and together with the 30S subunit crystal structures gave way to computational modeling studies of the assembly process.

First, Stagg et al. (36) explored the 3' assembly path using coarse-grained Monte Carlo simulated annealing technique. The one-bead per nucleotide and amino acid model was applied with harmonic interactions for pseudo-bonds, angles and torsions, and a volume exclusion term (37). Morse-like potential was used to represent specific protein-RNA interactions, which served as restraints to guide proteins to their appropriate binding sites. Additional pseudo atoms were added between RNA strands in helices to maintain their overall structure. The 16S rRNA starting model contained information only on its secondary structure. The 30S subunit proteins were sequentially added to the 16S RNA starting from a random position. Changes of fluctuations upon binding of proteins in the 3' domain (S7) path were assessed to predict the contributions of each protein to the organization of the binding sites. The authors found that the binding sites for primary binders are more ordered in the bare 16S RNA than the sites for other proteins. Therefore, binding of primary proteins reduces the flexibility of 16S rRNA and the primary binders also tend to organize the binding sites on RNA for later binders.

Another theoretical modeling of the 30S assembly map was based on the Poisson-Boltzmann model and calculations of the energetics of binding (12). The authors investigated the relative binding free energies of the 30S proteins to the 16S RNA in various orders to determine the most probable assembly path based on the energetics of binding. The electrostatic, nonpolar and entropic contributions to binding were taken into account. The Poisson-Boltzmann electrostatic energies were calculated on 300 processors of NPACI Data Star or 800 processors of Blue Horizon Supercomputers up to the 0.2Å grid resolution. The results demonstrated that for majority of proteins electrostatics opposes binding, even though all except one of the 30S proteins carries a positive net charge. This means that it is more favorable for proteins to interact with the high dielectric solvent than with the ribosomal RNA. Overall, the 5' domain proteins that bear the highest positive charge get buried the most upon binding to 16S rRNA, and are the strongest binders. A computationally derived binding affinity map was constructed, which classified the proteins according to the strength of interactions with the 16S rRNA and 30S subunit. Even though the map was only qualitative and based on relative binding free energies it

proved the ability of the computational models to be applied not only to single proteins and small ligands, but also to molecular assemblies composed of proteins and RNA.

To study the flexibility of 16S rRNA during binding of 30S proteins, Cui and Case (38) employed a similar to Stagg et al. (36) coarse-grained RNA and protein model, but used molecular dynamics technique. They performed multiple 100 ns long Langevin dynamics simulations and analyzed the conformational changes of 16S rRNA in the bound and unbound forms. The 3' domain i.e., the S7 assembly path was mainly studied, and the authors found structural explanations for the sequential binding of proteins in this path. The presence of primary and secondary proteins (S7 and S9) helps to organize the binding sites for tertiary proteins. Primary proteins help in stabilizing 16S rRNA, whose configuration while bare of proteins deviates significantly from the crystal structure, and acquire an extended-like form. If a tertiary protein is allowed to bind first, then the root mean square deviation of 16S rRNA is similar as in its unbound form. In the protein-bound 16S rRNA, the central domain is the most and the 3' minor domain the least stable.

The dependence of proteins on each other's binding to 16S rRNA was also studied with another reduced model (39). Each nucleotide and amino acid was represented as a single interacting center. The binding free energy was approximated by harmonic interactions along the backbones and within a certain cutoff distance. Bead-specific contact energy was also applied and the hamiltonian of the system was integrated by an analytic method. The approach focused on both changes in energetics and fluctuations. The interdependencies of protein binding were deduced by removing one or two proteins at a time from the full 30S complex. The binding free energies were computed as the difference between the energy of the complex and binding partners. The key proteins, most important in mutual stabilization were identified, and the stabilizing effect of each protein on the remaining ones was quantified. Non-local effects were found to be the cause of those influences. For example, proteins S15, S16, S20 and peptide Thx were found not to influence the binding of other proteins.

Recently, a similar dependence-based study was conducted (40), but was based on the dynamical effects derived from normal mode analysis. The 30S system was represented as an elastic network formed by Cα and P atoms connected by harmonic springs. The motions were analyzed based on anisotropic network model that takes into account the directionality of fluctuations and their anisotropy. The authors removed single proteins, pairs of proteins and various sets of proteins from the 30S complex and studied the effect of this removal on internal mobility of the remaining part of the 30S subunit. It turned out, that the motions of the 16S rRNA alone and inside the complete 30S subunit are very close. This means that the motion of the bare 16S rRNA is determined by its shape alone and that the intermolecular interactions between 16S rRNA and the 30S proteins do not affect the dynamics of 16S rRNA in the complex. The normal modes also predicted that proteins S6 and

S18 behave as one block which is in accord with previous studies showing that these two proteins bind as a dimer (32,33,39).

Up to date, no similar studies on the 50S subunit were performed. The reason is that the number of proteins in the 50S subunit is larger than in the 30S subunit and at least over 30 proteins would need to be classified. Moreover, the overall net charge of the large subunit is around -3000e, which makes this subunit a more difficult system to study with the known electrostatic models. The experimental approaches to the 50S subunit assembly are reviewed in (41).

7. Conclusions

Thanks to high resolution structures of the ribosome, various modeling approaches gave insight into ribosome function and dynamics. Studies of its internal dynamics determined both, the global collective motions and analyzed the details of the decoding process. Electrostatic calculations characterized the electrostatic potential around the ribosome. Various binding free energy techniques helped assess the energetics and kinetics of binding of antibiotics to the 30S subunit. Assembly paths of the 30S proteins were also derived. Despite the large size and high complexity of the ribosomal machine, all the molecular modeling efforts in the last years were proven to be useful and corroborated experimental data. However, modeling tools to be applicable to such nanoscale systems still need development. In future, computational modeling should definitely focus not only on the prokaryotic but also on the eukaryotic ribosomes, once atomic resolution structural data on the eukaryotic 80S ribosome become available.

Acknowledgements

The author acknowledges support from University of Warsaw (115/30/E-343/BST1345/ICM2008 and G31-4), Polish Ministry of Science and Higher Education (3 T11F 005 30, 2006-2008), Fogarty International Center (NIH Grant no R03 TW07318) and Foundation for Polish Science.

Literature

1. Liljas A., (2004), *Structural Aspects of Protein Synthesis*, World Scientific Publishing Co. Pte. Ltd.
2. Wimberly B. T., Brodersen D. E., Clemons Jr W. M., Morgan-Warren R. J., Carter A.P., Vonrhein C., Hartsch T., Ramakrishnan V., (2000), Nature, 407, 327-339.
3. Schluenzen F., Tocilj A., Zarivach R., Harms J., Gluehmann M., Janell D., Bashan A., Bartels H., Agmon I., Franceschi F., Yonath A., (2000), Cell, 102, 615-623.
4. Ban N., Nissen P., Hansen J., Moore P. B., Steitz T. A., (2000), Science, 289, 905-920.
5. Yusupov M. M., Yusupova G. Z., Baucom A., Lieberman K., Earnest T. N., Cate J. H. D., Noller H. F., (2001), Science, 292, 883-896.
6. Bernstein F. C., Koetzle T. F., Williams G. J. B., Meyer J. E. F., Brice M. D., Rodgers J. R., Kennard T. S., Tasumi M., (1977), J. Mol. Biol., 112, 535-542.

7. Honig B., Nicholls A., (1995), Science, 268, 1144-1149.
8. Baker N. A., (2004), *Poisson-Boltzmann methods for biomolecular electrostatics*, in: *Methods in Enzymology*, Elsevier Inc., USA, 383, 94-118.
9. Baker N. A., Sept D., Joseph S., Holst M. J., McCammon J. A., (2001), Proc. Natl. Acad. Sci. USA, 98, 10037-10041.
10. Gabashvili I. S., Agrawal R. K., Grassucci R., Squires C. L., Dahlberg A. E., Frank J., (1999), EMBO J, 18, 6501-6507.
11. Frank J., Agrawal R. K., (2000), Nature, 406, 318-322.
12. Trylska J., Tozzini V., McCammon J. A., (2005), Biophys. J., 89, 1455-1463.
13. Tung C. S., Sanbonmatsu K. Y., (2004), Biophys. J., 87, 2714-2722.
14. Sanbonmatsu K. Y., Joseph S., Tung C. S., (2005), Proc. Natl. Acad. Sci. USA, 44, 15854-15859.
15. Mehta R., Champney W. S., (2002), Antimicrob. Agents and Chem., 46, 1546-1549.
16. Ma C., Baker N. A., Joseph S., McCammon J. A., (2002), J. Am. Chem. Soc., 124, 1438-1442.
17. Massova I., Kollman P. A., (2000), Perspect Drug Discovery, 18, 113-135.
18. Yang G., Trylska J., Tor Y., McCammon J. A., (2006), J. Med. Chem., 49, 5478-5490.
19. Dlugosz, M., Trylska, J., submitted.
20. Valle M., Zavialov A., Sengupta J., Rawat U., Ehrenberg M., Frank J., (2003), Cell, 114, 123-134.
21. Chacon P., Tama F., Wriggers W., (2003), J. Mol. Biol., 326, 485-492.
22. Tama F., Valle M., Frank J., Brooks III C. L., (2003), Proc. Natl. Acad. Sci. USA, 100, 9319-9323.
23. Wang Y., Rader A. J., Bahar I., Jernigan R. L., (2004), J. Struct. Biol., 147, 302-314.
24. Gavrilova L. P., Kostiashkina O. E., KotelianskyV. E., Rutkevitch N. M., Spirin A. S., (1976), J. Mol. Biol., 101, 537-552.
25. Southworth D. R., Brunelle J. L., Green R., (2002), J. Mol. Biol., 324, 611-623.
26. Sanbonmatsu K. Y., Tung C. S., (2007), J. Struct. Biol., 157, 470-480.
27. Lu J. L., Deutsch C., (2005), Nat. Struct. Mol. Biol., 12, 1123-1129.
28. Ziv G., Haran G., Thirumalai D., (2005), Proc. Natl. Acad. Sci. USA, 102, 18956-18961.
29. Kirmizialtin S., Ganesan V., Makarov D. E., (2004), J. Chem. Phys., 121, 10268-10277.
30. Elcock A. H., (2006), PLoS Comp. Biol., 2, 0824-0841.
31. Go N., (1983), Annu. Rev. Biophys. Bioeng., 12, 183-210.
32. Held W. A., Ballou B., Mizushima S., Nomura M., (1974), J. Biol. Chem., 249, 3103-3111.
33. Powers T., Daubresse G., Noller H. F., (1993), J. Mol. Biol., 232, 362-374.
34. Talkington M. W. T., Siuzdak G., Williamson J. R., (2005), Nature, 438, 628-632.
35. Williamson J. R., (2008), Curr. Opin. Struct. Biol., 18, 299-304.
36. Stagg S. M., Mears J. A., Harvey S. C., (2003), J. Mol. Biol., 328, 49-61.
37. Malhotra A., Tan R. K.-Z., Harvey S. C., (1994), Biophys. J, 66, 1777-1795.
38. Cui Q., Case D. A., (2006), Multiscale Model Simul., 5, 1248-1263.
39. Hamacher K., Trylska J., McCammon J. A., (2006), PLoS Comp. Biol., 2, 0080-0087.
40. Yan A. M., Wang Y. M., Kloczkowski A., Jernigan R. L., (2008), J. Chem. Theo. Comput., 4, 1757-1767.
41. Klein D. J., Moore P. B., Steitz T. A., (2004), J. Mol. Biol., 340, 141-177.